An efficient and robust simulator for wear of total knee replacements

Ansgar Burchardt[1], Christian Abicht[2] and Oliver Sander[1]

Abstract

Wear on total knee replacements is an important criterion for their performance characteristics. Numerical simulations of such wear have seen increasing attention over the last years. They have the potential to be much faster and less expensive than the in vitro tests in use today. While it is unlikely that in silico tests will replace actual physical tests in the foreseeable future, a judicious combination of both approaches can help making both implant design and pre-clinical testing quicker and more cost-effective. The challenge today for the design of simulation methods is to obtain results that convey quantitative information and to do so quickly and reliably. This involves the choice of mathematical models as well as the numerical tools used to solve them. The correctness of the choice can only be validated by comparing with experimental results. In this article, we present finite element simulations of the wear in total knee replacements during the gait cycle standardized in the ISO 14243-1 document, used for compliance testing in several countries. As the ISO 14243-1 standard is precisely defined and publicly available, it can serve as an excellent benchmark for comparison of wear simulation methods. We use comparatively simple wear and material models, but we solve them using a new wear algorithm that combines extrapolation of the geometry changes with a contact algorithm based on nonsmooth multigrid ideas. The contact algorithm works without Lagrange multipliers and penalty parameters, achieving unparalleled stability and efficiency. We compare our simulation results with the experimental data from physical tests using two different actual total knee replacements. Even though the model is simple, we can predict the total mass loss due to wear after 5-million gait cycles, and we observe a good match between the wear patterns seen in experiments and our simulation results. When compared with a state-of-the-art penalty-based solver for the same model, we measure a roughly fivefold increase of execution speed.

Introduction

The wear between tibial plateau and femoral component is one of the main limiting factors for the life-span of total knee replacements (TKRs). In the course of millions of gait cycles, the hard (cobalt–chrome) femoral condyles grind off small particles from the tibial plateau, which is usually made from relatively soft polyethylene (ultra-high-molecular-weight polyethylene (UHMWPE)). Small microparticles start to migrate within the knee joint, leading to inflammation and eventually osteolysis.[1] In extreme cases, mechanical failure of the (surface of the) tibial plateau has been observed for gamma-sterilized implants.[2]

To limit these risks, various national guidelines require pre-clinical in vitro testing of the wear behavior of knee implants. These tests are performed by knee wear testing machines. The precise conditions are formulated in a series of documents published by the International Organization for Standardization (ISO). We focus here on ISO 14243-1,[3] which describes testing conditions of a load-controlled testing gait cycle for normal walking. A wear test consists of 5 million such cycles, and of monitoring the mass loss of the tibial bearing component.

Performing such experimental tests is a cost-intensive task. The required 5-million cycles take about 3 months

[1]Institut für Numerische Mathematik, Technische Universität Dresden, Dresden, Germany
[2]Questmed GmbH, Kleinmachnow, Germany

Corresponding author:
Oliver Sander, Institut für Numerische Mathematik, Technische Universität Dresden, 01062 Dresden, Germany.
Email: oliver.sander@tu-dresden.de

of time. The initial positioning of the femoral and tibial components with respect to each other is not precisely specified by ISO 14243-1 for all cases. Its determination remains an important open problem for wear testers and designers of knee implants.[4,5]

Computer simulations of these standardized tests can help to reduce costs and time-to-market. While simulations cannot replace the actual compliance tests, they can help to avoid some of the preliminary tests that need to be performed during the design phase of a new implant. In particular, numerical simulations can help to determine suitable initial configurations. With this information, the number of actual physical experiments is greatly reduced.

For these reasons, the numerical simulation of TKR wear behavior has seen increasing interest over the past years. Various finite element and rigid body models appear in the literature, all combining different contact formulations and wear laws. While some authors consider Archard's wear law to be sufficient,[6,7] others focus on developing more advanced laws to better capture the behavior of UHMWPE.[8,9] Several groups use the ISO 14243 test family as a benchmark problem,[7,10] but only the latter group uses the load-controlled variant 14243-1. Abdelgaied et al.[8] and O'Brien et al.[9] compared their findings with experimental results. Grupp et al.[11] apply simulations to investigate the effects of different material properties of TKRs for different activities, see also Abdelgaied et al.[12] Finally, Kang et al.[13] performed simulations similar to ours, but with an off-the-shelf penalty solver, and report simulation times in the range of 1 week.

In this contribution, we consider a finite element model of two TKRs including the tibial inlay and femoral component. Following Abicht[14] and Willing and Kim,[7] we model both components as deformable objects because numerical tests showed that surprisingly little run time can be saved by keeping the femoral component rigid. We model the contact between the two objects exactly, with a surface-to-surface (mortar) discretization[15,16] without recourse to any regularization parameter. The wear on the tibial plateau is described using Archard's wear law. We compare the predicted wear patterns and total wear mass loss to values obtained by experimental testing.

The main contribution of this article is the introduction of a new algorithm for the simulation of wear, which combines the extrapolation of the geometry changes with a globally convergent, penalty-free contact solver algorithm. The combined robustness and speed of that algorithm allow to compute wear predictions in less time (in the range of hours) and with less manual intervention. Numerical wear testing requires the solution of many contact problems, in particular, if long-time wear, statistical effects or shape-optimization is involved. Most articles mentioned above use commercial finite element software, which typically uses penalty approaches or augmented Lagrangian methods for the contact problems. These methods have well-known drawbacks. Penalty methods do allow a bit of nonphysical penetration. Choosing a large penalty parameter diminishes the penetration, but the problem may become unstable. A suitable penalty factor is a compromise, and usually only obtained after a few steps of trial and error. Augmented Lagrangian methods, however, need to solve each problem several times. In addition, the number of variables increases, as the method needs to track approximations of the contact forces (see, for example, Chap. 8.4 in the study by Maas et al.[17] for a discussion).

In contrast, our contact model uses a novel nonsmooth optimization algorithm which solves the contact problems directly.[18] It uses a sparse direct solver for its linear correction steps, but performs the costly matrix factorization only once per contact problem. This avoids all the above-mentioned drawbacks—instead, the solver is provably convergent,[18] and it does not involve additional Lagrange multiplier variables or penalty parameters. It is the goal of this article to demonstrate that this solver can lead to shorter simulation times for TKR models of reasonable complexity. Generalization of the method to more advanced models will be the subject of future work. For example, recent work[19] has shown that a similar algorithm performs well for small-strain elastoplastic materials. The combination of this with contact and wear appears as a natural next step.

Previous versions of the contact simulator have been used in earlier work on biomechanics,[20–22] but the extension to wear problems is new. In the cited works, larger grids were considered, which required the use of multigrid techniques. The nontrivial use of direct solvers without refactorization proposed here is new.

Methods

We simulated the ISO 14243-1 testing cycle using a finite element model that included both the femoral component and the tibial inlay of the implant as deformable bodies. The two interacted by a contact condition which we modeled using a surface-to-surface (mortar) contact discretization.[15,16] As TKRs are well lubricated inside the testing machine, and as Archard's wear law does not involve the tangential stresses, we omitted friction from the contact model. The numerical code was our own research implementation based on the C++ open-source finite element code Dune.[23–25]

Finite element model

We tested our simulation procedure with two implants that are sold commercially, and for which all geometry data and the original experimental results of the ISO 14243-1 compliance testing were gratefully made available to us by the manufacturer (aap Implantate GmbH, Berlin, Germany). These are a "Mebio 2015" (in the following: Mebio)[26] and a "Genius Pro, Fixed Bearing, posterior cruciate ligament (PCL) retaining" (in the
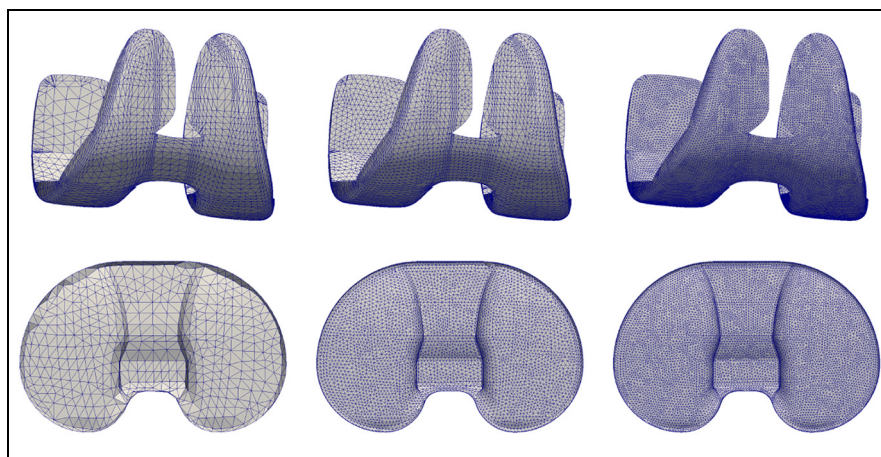
Figure 1. Tetrahedral meshes 1–3 (from left to right) for femoral and tibial components of the Mebio implant.
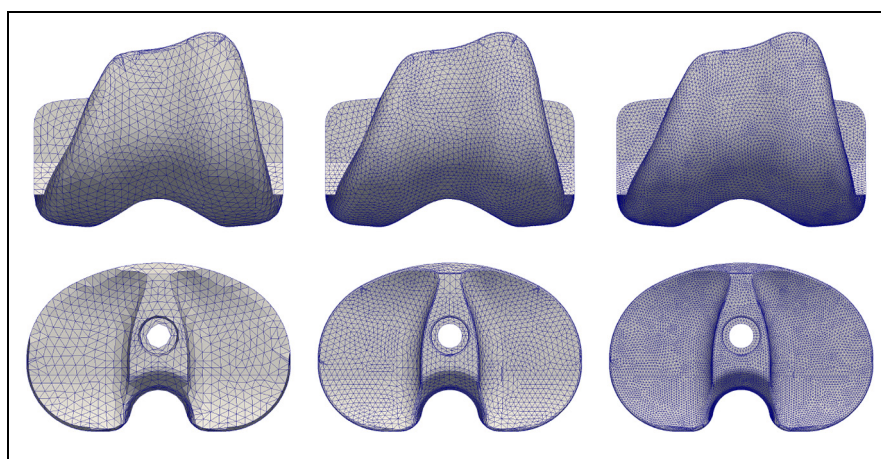
Figure 2. Tetrahedral meshes 1–3 (from left to right) for femoral and tibial components of the Genius Pro implant.

following Genius Pro).[27] More details are given in the section on physical wear tests. Computer-aided design (CAD) data of the TKR volumes were available in Parasolid format. Tetrahedral volume meshes with different resolutions were constructed using ANSYS (ANSYS Inc., Canonsburg, PA, USA) and the open-source mesh generator GMSH.[28] The meshes for the tibial components had between 5000 and 120,000 elements (1500–26,500 nodes) for the Genius Pro implant, and between 4000 and 190,000 elements (1200–38,000 nodes) for the Mebio implant, see Table 1. Four-node tetrahedral finite elements were used for the discretization.

To simplify the mesh construction, the geometries of the implants were simplified slightly on their rear sides. The geometric modifications did not involve areas close to the contact region. Geometric changes this far away from the contact surface do not have a relevant influence on the wear behavior. Figure 1 shows the meshes used for the Mebio implant; Figure 2 shows the ones used for the Genius Pro implant.

The UHMWPE of the tibial inlay as well as the cobalt–chromium–molybdenum alloy of the femoral

Table 1. Mesh resolutions.

Mesh	Number of elements	Number of nodes
Mebio 1		
Femur	13,824	4633
Tibia	3948	1205
Mebio 2		
Femur	31,432	9234
Tibia	81,400	17,445
Mebio 3		
Femur	184,526	42,750
Tibia	188,993	37,982
Genius Pro 1		
Femur	9238	2820
Tibia	4720	1496
Genius Pro 2		
Femur	33,864	8745
Tibia	18,799	5038
Genius Pro 3		
Femur	109,045	24,550
Tibia	121,548	26,484

For each of the two TKRs, meshes in three different resolutions were constructed.
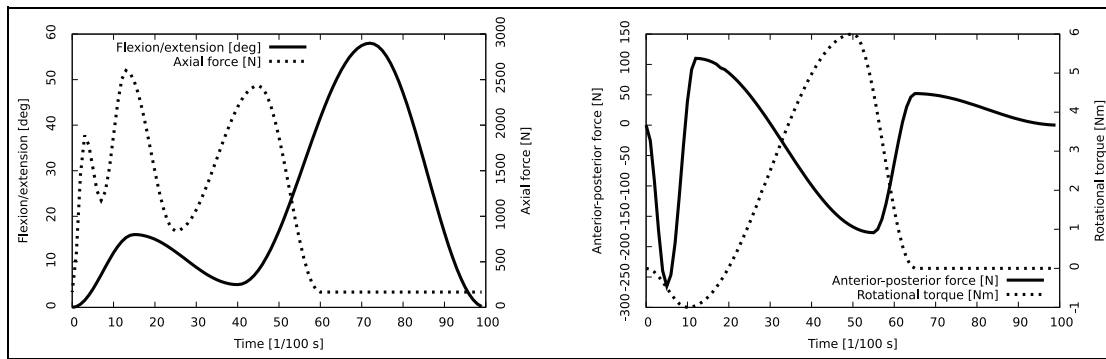
Figure 3. Left: Loading conditions during the gait cycle as prescribed by ISO 14243-1. Flexion/extension displacement boundary conditions applied to the femoral component, and axial force applied to the tibial component. Right: Anterior–posterior force and rotational torque applied to the tibial component.

component was modeled as homogeneous and isotropic materials, with linear elastic stress–strain relationships. Material parameters were taken from Abicht[14] (p. 51). (The particular type of polyethylene used there was UHMWPE standard Chirulen GUR 1020. It was Gamma-sterilized, and not cross-linked.) Young's modulus $E = 220$ GPa and Poisson's ratio $\nu = 0.31$ were used for the femoral component, and values $E = 1.1$ GPa, $\nu = 0.42$ were used for the tibial inlay. Both Poisson's ratios are far away from the incompressibility limit at $\nu = 0.5$, and there was therefore no danger of Poisson locking, that is, excessive model stiffness, even for four-node tetrahedral elements.[29]

The reference position for the femoral and tibial inlay meshes was determined by manually applying a translation to the tibial component in a visualization tool such that the most distal points on the femoral component rested on the lowest point on the tibial side.

Time-dependent boundary conditions were set as described by the ISO 14243-1 standard. The standard describes a single gait cycle by giving a table listing boundary values for 100 discrete time steps within one gait cycle. The flexion/extension movement of the femoral component is controlled by a time-dependent displacement boundary condition applied to all nodes of the component backside (Figure 3). The boundary conditions for the tibial inlay are slightly more complicated:

- The main load is an axial force pushing the tibial side upward against the femoral component, with time-dependent values between 167.6 and 2600 N.
- A smaller force acts on the inferior side of the tibial inlay in anterior–posterior direction with values between −265 and 110 N.
- An internal–external torque around the axis of the axial force is applied, with values between −1 and 6 N m.

These loads were applied as surface loads over the entire inferior side of the tibial component (Figure 4). In addition, the inlay was kept in place by restraining
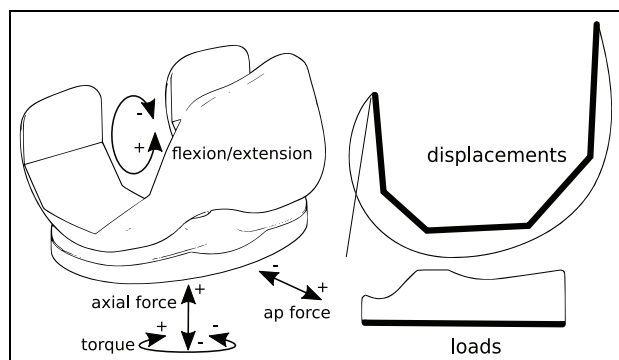
Figure 4. Left: Axes for the different boundary conditions, as prescribed by ISO 14243-1. Right: The boundary conditions are enforced on the superior side of the femoral component and the inferior side of the tibial inlay. All forces are applied as surface loads.

forces and torques that penalize anterior–posterior displacement and internal–external rotation. These forces and torques were proportional to the anterior–posterior displacement and tibial rotation, respectively. They were modeled as Robin (i.e. spring-type) boundary conditions on the inferior side of the tibial inlay. Note that this testing cycle was load controlled, and no displacement boundary condition was applied to the tibial side at all. Rigid-body motion of the tibial inlay was avoided solely by the femoral contact together with the upward force on the inlay, and the restraining forces and torques modeled as Robin boundary conditions. Mathematically, the resulting problems were well-posed, but have rank-deficient system matrices, making the finite element system challenging to solve.

For simplicity, we have assumed a linear stress–strain relationship for UHMWPE. Nevertheless, the partial differential equations describing the elastic behavior of a full gait cycle remain nonlinear, because the testing movement involves large rotations, which require a nonlinear strain tensor to be handled properly. We avoided having to solve nonlinear equations by noting that the movement of the model consists of

rotations superimposed by only small deformations. The rotations are known a priori—they are described by the femoral component displacement boundary conditions. These boundary conditions were therefore used to create a sequence of time-dependent reference domains, and we solved for the small deformations only. This permitted to use a linear strain tensor and to solve a sequence of 100 linear contact problems on changing reference domains instead of nonlinear ones on a fixed domain. As the model does not include inertia or rate effects, the results of these 100 problems were independent of each other and could be computed in parallel using OpenMP.[30]

We modeled the contact between the two objects by a penalty-free surface-to-surface (mortar) finite element discretization as described by Wohlmuth and Krause.[31] Mortar discretization avoid the unphysical stress oscillations that are known to occur in node-to-node contact methods.[15] We omitted friction effects because we modeled a situation where the TKR is well lubricated, and because according to Archard's law, wear depends only on normal stresses, whereas friction primarily impacts tangential stresses.

The resulting systems of equations were solved using a nonsmooth multigrid method[32] together with a sparse direct solver for the linear correction steps. This solver is guaranteed to converge to the solution in all cases,[18] without the need for artificial load stepping. The stiffness matrix was factorized only once per time step, and line/column truncations of the matrix were applied via fast low-rank updates. The method is parameter free, meaning that there are no additional values that would need proper tuning to make the algorithm function properly. The contact problems were solved up to a relative accuracy of 10^{-8} for the displacement fields. Extension of the solver to include certain friction laws is possible.[18,33]

Wear and grid deformation

We used Archard's wear law[34] to model the wear on the tibial inlay. For each point on the contact surface, Archard's law models the wear depth l at that point. The wear depth at a time t is given by

$$l(t) = k \int_0^t |p(t)v(t)| dt \qquad (1)$$

where k is a material constant, p is the contact pressure at this point and v is the relative velocity between the two objects. If p is independent of time, and the sliding velocity is constant, then we obtain the formula

$$l = kps$$

with the sliding distance s typically seen in the literature. However, these assumptions clearly do not hold

in finite element TKR simulations, and our code therefore implements the general integral formula (1). Total volume loss was computed as the integral of l over the contact surface. Pressure p and current velocity v were computed from the finite element model. For the wear constant k, we chose the value 2.0×10^{-7} mm^3/N m, used by O'Brien et al.[9] in a simulation of wear in TKRs using Archard's wear law. This is an important point: we did not use the experimental data available to us to determine the important wear coefficient k.

Even with a fast numerical solver, solving the 100 time steps for each of the 5-million gait cycles mandated by ISO 14243-1 is not possible. However, Archard's wear law depends on the wear history only indirectly through the change in geometry. This change will be small in a single gait cycle, and we therefore ignored it and extrapolated the wear values obtained for a single gait cycle over a larger number of cycles. We estimated the wear over n_Δ cycles by extrapolating the wear of a single gait cycle linearly, that is, by multiplying l by n_Δ. To obtain a reasonable value for the cycle step size n_Δ, we performed simulations on one grid per implant and compared the total wear loss over time for different choices of n_Δ between 2×10^4 and 2×10^5.

Linear extrapolation works over numbers of gait cycles that are not too large. However, when very large numbers of cycles are considered, the change in geometry needs to be taken into account. This change will be hardly noticeable on the femoral component, but very relevant on the softer tibial inlay. As Archard's law does not indicate the distribution of wear between two materials of differing hardness, we assumed all wear to happen on the tibial inlay. Therefore, after each n_Δ gait cycles, we deformed the tibial grid by adding the extrapolated wear depth in normal direction to the grid contact surface. From then on, this modified geometry was used as the reference configuration for the subsequent simulation steps. Also, we used this deformed grid to recompute the normal field for the next geometry update. As the wear depth l is small, adding it to the grid hardly influences the grid quality at all. To be on the safe side, after changing the grid boundary, we performed a grid smoothing step. Similar to Laplace smoothing, we solved a linear elastic problem for the tibial inlay with the wear depth l multiplied by the surface normal direction as displacement boundary condition. The computed displacements at the inner nodes were then applied to the grid.

Combining finite element simulations, linear extrapolation and grid deformation lead to the following hybrid time-stepping method to compute long-time wear patterns and mass loss. An extrapolation step size n_Δ is picked and the following three steps are performed:

1. Compute surface wear for a single gait cycle.
2. Multiply the result by n_Δ to obtain the extrapolated values for n_Δ gait cycles.
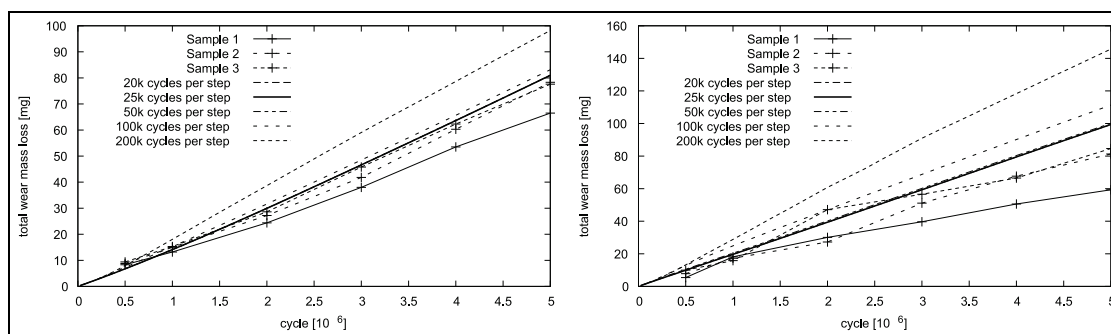
Figure 5. Total wear mass loss as a function of time for different extrapolation step sizes n_Δ (left: Mebio; right: Genius Pro). Lines without symbols represent simulated data; the other ones represent experimental data. The lines for 20,000, 25,000 and 50,000 gait cycles per extrapolation step are overlapping, which indicates that an extrapolation step length of $n_\Delta = 5 \times 10^4$ (50,000) is a good compromise between accuracy and execution speed.

3. Modify geometry using the extrapolated wear depth.

These three steps are repeated until the total number of gait cycles reaches 5 million. The result is the total mass loss due to wear over time, and the wear patterns in the tibia that can be read off directly from the grid.

Physical wear tests

Physical wear testing data were kindly provided by the manufacturer aap Implantate AG (Berlin, Germany), and by Questmed GmbH (Kleinmachnow, Germany), an accredited test laboratory for physical testing of implants. No dedicated tests were performed for this study, but rather we were allowed to use the data from the original compliance tests.

The data set contained wear results for two types of TKRs, both manufactured by aap Implantate AG (Berlin, Germany). The first was a MebioKnee system TR 15-046, with a size S, height 7.5 tibial inlay and size S cobalt–chrome–molybdenum (ISO 5832-4) tibial inlay and femoral components ("Mebio"). The other one was a Genius Pro Fixed Bearing, PCL retaining TKR system, with a size M, height 6.5 tibial inlay, and size M tibial inlay and femoral components ("Genius Pro"). The polyethylene used in these experiments was UHMWPE standard Chirulen GUR 1020. It was Gamma-sterilized, and not cross-linked.

The implants were tested according to the specification of the ISO 14243-1 wear testing standard. Three identical implants of each type were tested in parallel, under identical conditions. Total mass loss was measured every 5×10^5 cycles. After the wear testing, the wear results on each tibia inlay were photographed. The relative area of the wear marks was evaluated by manually segmenting the marks and counting pixels.

Results

We performed two sets of tests. The first set compared simulated wear rates and patterns with experimental data. This is mainly to check that we calibrated the model well. The more important second set of tests demonstrates that our algorithm solves the resulting problems much faster than penalty-based ones.

Wear prediction

Figure 5 shows the result of the convergence study for the extrapolation step length n_Δ. The values indicate that $n_\Delta = 5 \times 10^4$ is a good choice.

Figure 6 shows the total mass loss due to wear after up to 5-million gait cycles for the two implant geometries. The three sets of experimental data are shown for each implant. For both implant types, there are two sets of data that agree very well with each other, whereas the third one shows lower values (10% for the Mebio implant and 25% for the Genius Pro implant).

The simulation predicts 98.31/81.04/53.13 mg of mass loss for the Mebio for the three grids, and 112.18/100.15/98.44 mg for the Genius Pro after 5 million cycles. This matches the corresponding experimental results in the range of 66.5–77.6 mg for the Mebio, and between 59.33–84.65 mg for the Genius Pro well. We observe that mass loss for the Genius Pro implant appears to converge for increasing mesh resolution, whereas the corresponding number for the Mebio implant does not. This highlights the difficult nonlinear nature of the contact/wear problem. We also observe that the experimental curves start with a steeper slope that flattens after about 1-million gait cycles, an effect that is not reproduced by the simulation.

Figures 7 and 8 show the simulated wear patterns for both implants. For the Mebio implant, sizes, shapes and positions of the wear marks match the corresponding experimental results very well, as can be seen in the overlay in Figure 9. Wear occurs on 12.5%–15.6% of the proximal side of the tibial inlay in the simulation compared to 13.7%–16.5% in the experiment. The experimental wear pattern of the Genius Pro implant shows several secondary wear marks near the border of the tibial plateau (Figure 10). These are typical for this type of implant, and they are caused by anterior–posterior
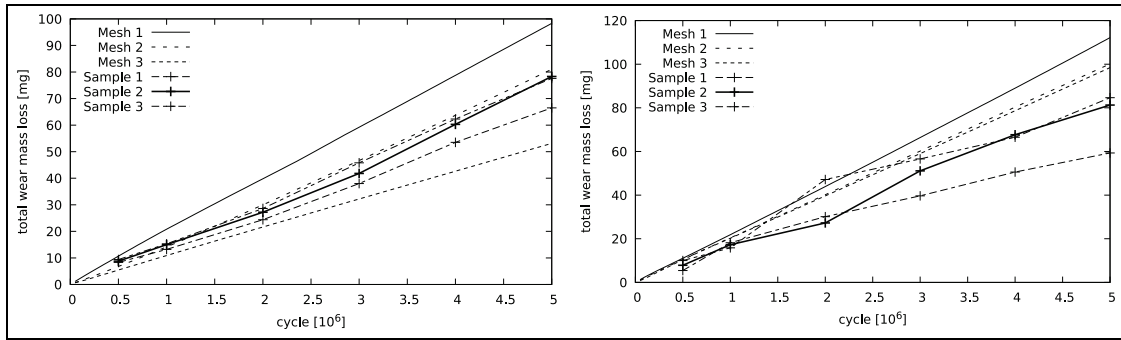
Figure 6. Experimental versus simulated wear mass loss for the Mebio (left) and Genius Pro (right) implants. The experimental results were taken at intervals of 1-million gait cycles. The geometry was adapted every $n_\Delta = 5 \times 10^4$ gait cycles.
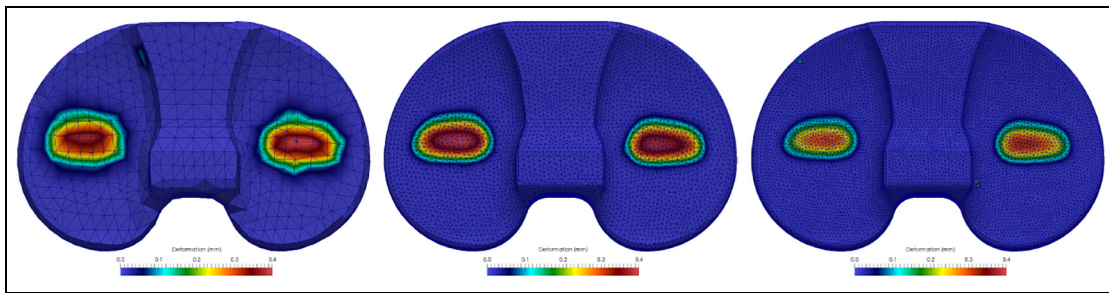
Figure 7. Spatial distribution of wear for the Mebio implant for the three grid resolutions shown in Figure 1, with resolutions given in Table 1 (left: coarsest; right: finest). Color denotes the wear depth.
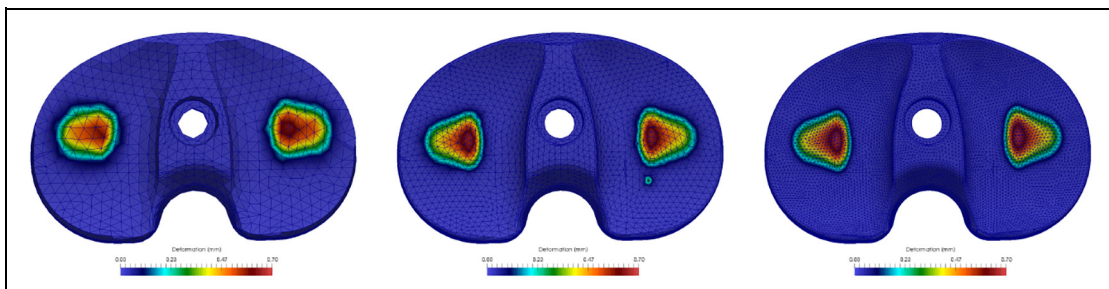
Figure 8. Spatial distribution of wear for the Genius Pro implant for the three grid resolutions shown in Figure 2, with resolutions given in Table 1 (left: coarsest; right: finest). Color denotes the wear depth.
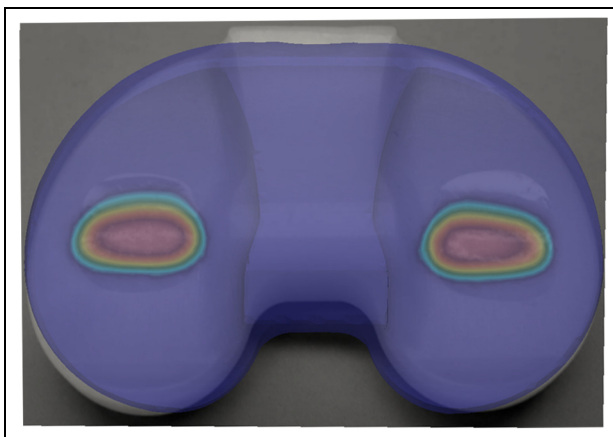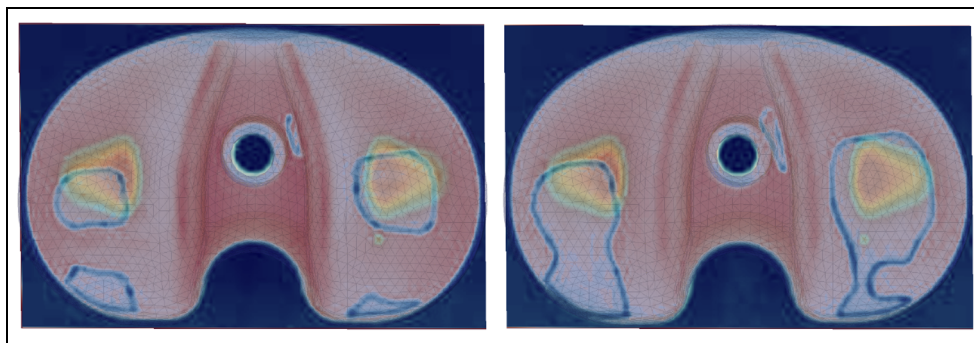

Figure 9. Overlay of simulated and experimental wear for Mebio implant after 5-million gait cycles, with the finest grid and extrapolation step length $n_\Delta = 5 \times 10^4$.

translations in the swing phase. The numerical simulation does not show these marks. The main wear marks do not appear quite at the positions of the experimental ones. Wear occurs on approximately 10% of the surface in the simulation; on the experimental side, the area is much larger (about 20%). From the distribution, one can see that the numerical simulation does not resolve the increase of the wear area due to anterior–posterior movement.

The simulation also makes precise predictions about the wear depth at each point on the tibial surface. However, no comparison data were available.

Computational efficiency

The solver algorithm displays considerable efficiency improvements compared to state-of-the-art solvers. As

Figure 10. Overlay of simulated and experimental wear for Genius Pro implant after 5-million gait cycles. The wear marks on the edges of the implant are typical in this type. They are caused by anterior–posterior translations in the swing phase.

Table 2. Wall-time comparison between nonsmooth multigrid solver and state-of-the-art interior-point solver Ipopt for the time needed to compute the wear during one of the 100 substeps of the gait cycle of ISO 14243-1.

Mesh	Assembly time (s)	Solve (Ipopt)	Solve (nonsmooth contact)
Mebio 1	0.8	1.2	1.1
Mebio 2	6.7	75.6	16.3
Mebio 3	21.2	687.3	103.3
Genius Pro 1	0.6	2.3	1.1
Genius Pro 2	2.3	19.6	5.7
Genius Pro 3	12.2	253.4	66.7

As the 100 substeps are all independent of each other, they can be distributed across a multi-processor machine.

the time needed to evaluate Archard's wear law (1) and the geometry deformation were negligible compared to solving the contact problems, our test focused on these latter problems. Table 2 shows the wall time needed to solve one contact problem on each of the six meshes of Figures 1 and 2. Wall times are given for the nonsmooth multigrid method as well as for the Ipopt solver,[35] which we used as a reference. Ipopt is a widely used interior-point solver, that is, a penalty method with automatic control of the penalty parameter. The nonsmooth multi-grid method is consistently faster by a factor of 4–6.

When using a single processor (Intel Xeon E5-2680, 2.5 GHz), the total simulation on medium-sized meshes with 12,000–14,000 degrees of freedom in total took 16.3–19.2 h. By far, the majority of time was spent solving the contact problems.

As the 100 contact problems of a single gait cycle can be computed independently from each other, it is straightforward to distribute them across several processors. The contact problems take the majority of the run time, and therefore, we expect almost linear scaling for up to 100 processors. Indeed, when repeating the simulations with 10 processors, the simulation took only between 2.5 and 2.9 h. This is a speed-up of about 6.5 compared to the single-processor run.

Discussion

While numerical simulations are not yet reliable enough to completely replace in vitro pre-clinical testing, they nevertheless have the potential to reduce the number of tests in the design and pre-clinical phase, thereby reducing development costs and time-to-market.

As a particular example, note that the ISO 14243-1 document does not completely specify the initial mutual positioning and orientation of the femoral and tibial TKR parts, because, by necessity, they are somewhat design dependent. However, the initial positioning is something that even the manufacturer needs to determine by experimental testing. Here, numerical tests can be of great help, as they allow to cheaply check whether a given position is reasonable.

A standard ISO 14243-1 test simulating 5-million gait cycles takes about 3 months to complete. It is no particular challenge to construct finite element models that compute approximate wear marks and mass loss in less time than that. Nevertheless, it is desirable to have computer codes that are as fast as possible. The less time is needed for an in silico estimation of the wear behavior of a particular TKR, the better this information can be integrated into the design process. This is where our wear simulation algorithm excels. A complete simulation with $n_\Delta = 5 \times 10^4$ takes only about 22–30 h on a single processor. Even better, it scales almost linearly with the number of processors available (up to 100, because that is the number of substeps in the ISO 14243-1 gait cycle specification). As multi-processor machines have become cheap and commonplace over the years, there is no problem to obtain wear results for a complete test in even under half an hour. As a further bonus, our nonsmooth contact algorithm is guaranteed to produce the correct solution of the mathematical model in all situations.[18] No fine-tuning of load-stepping parameters or similar human intervention is necessary. The algorithm runs completely autonomous. This saves precious human resources.

Furthermore, rapid numerical simulations open new possibilities even early in the design process. The impact of different variants of the implant shape on the wear behavior can be assessed without ever constructing a

physical prototype. Modern mathematical techniques known as shape-optimization even allow to create optimal shapes automatically.[7,36] However, such methods can only be used in practice if a fast and reliable simulation tool for wear is available.

Evaluation of the numerical results is difficult because only three data sets were available for each of the two implant types. Even the different physical results for a single implant type vary, which highlights the sensitivity of the experimental studies to input imperfections. At the same time, the assumptions of linear stress–strain relationship for UHMWPE, frictionless contact and Archard's wear law are all fairly restrictive. Therefore, only rough quantitative agreement can be expected. The results show, however, that a numerical simulation with the given simple model can produce quantitative results of the wear on a TKR during an ISO 14243-1 testing cycle that are close to the results obtained by actual experiments.

While the model achieves a rough agreement with experimental data, it is obviously too simple to explain the observed effects in detail. A natural next step would be to replace the elastic material of the tibial component by an elastoplastic one, which may do away with some of the wear mark discrepancies seen in Figures 9 and 10. Indeed, using recent results on solvers for elastoplastic materials,[19] it should be natural to extend the algorithm presented here also to wear simulations of elastoplastic materials.

Archard's wear law is the simplest one in a list of different models for mechanical wear. It is shown to give reasonably accurate results in many situations.[6,7] Other wear laws try to take into account additional material properties such as cross-shearing, creep or dependency of the wear factor on contact pressure,[8,9,37–39] but none of them could be established as a standard so far. O'Brien et al.[9] compare six different wear models and obtain good results using Archard's law.

Our own results also show that Archard's law is sufficient to obtain reasonable estimates of the overall wear rate. With this goal met, we can benefit from its advantages. The most important one is that Archard's law contains only one unknown parameter, the wear coefficient k. We were able to pick a good parameter value from the literature, without any recourse to the TKR experimental data available to us. More precise values of the wear coefficient k also depend on factors like the precise material and the method used to sterilize it. However, in production situations, this is not a problem, as k can be measured easily in separate experiments. More advanced wear laws would require additional parameters, which are in general not easy to obtain. Some laws additionally include internal states for which separate differential equations need to be solved. With such a wear law, we would lose the ability to compute the hundred time steps of one gait cycle in parallel, sacrificing a lot of computational performance.

Not surprisingly, Archard's law does not reproduce the observed effect that the experimental curves start with a steeper slope that flattens after about 1-million gait cycles. The presumed cause for this is that unused implants have a rougher surface, which becomes smoother after an initial number of cycles. Surface smoothness could be integrated easily into our model using an iteration-dependent wear coefficient k, rather than keeping k fixed as in the classical Archard's law. In any case, the overall effect seems to be negligible.

Declaration of conflicting interests

Funding

ORCID iD

Oliver Sander https://orcid.org/0000-0003-1093-6374

References

1. Gupta SK, Chu A, Ranawat AS, et al. Review article: osteolysis after total knee arthroplasty. *J Arthroplast* 2007; 22: 787–799.
2. Brandt JM, Medley J, MacDonald S, et al. Delamination wear on two retrieved polyethylene inserts after gamma sterilization in nitrogen. *Knee* 2011; 18(2): 125–129.
3. ISO 14243-1:2009. Implants for surgery: wear of total knee-joint prostheses—part 1: loading and displacement parameters for wear-testing machines with load control and corresponding environmental conditions for test.
4. Mell SP, Wimmer MA and Lundberg HJ. The choice of the femoral center of rotation affects material loss in total knee replacement wear testing: a parametric finite element study of ISO 14243-3. *J Biomech* 2019; 88: 104–112.
5. Brockett C, Abdelgaied A, Haythornthwaite T, et al. The influence of simulator input conditions on the wear of total knee replacements: an experimental and computational study. *Proc IMechE, Part H: J Engineering in Medicine* 2016; 230(5): 429–439.
6. O'Brien S, Luo Y, Wu C, et al. Computational development of a polyethylene wear model for the articular and backside surfaces in modular total knee replacements. *Tribol Int* 2013; 59: 284–291.
7. Willing R and Kim IY. Three dimensional shape optimization of total knee replacements for reduced wear. *Struct Multi Optim* 2009; 38(4): 405–414.

8. Abdelgaied A, Liu F, Brockett C, et al. Computational wear prediction of artificial knee joints based on a new wear law and formulation. *J Biomech* 2011; 44: 1108–1116.

9. O'Brien ST, Bohm ER, Petrak MJ, et al. An energy dissipation and cross shear time dependent computational wear model for the analysis of polyethylene wear in total knee replacements. *J Biomech* 2014; 47: 1127–1133.

10. O'Brien S, Luo Y, Wu C, et al. Prediction of backside micromotion in total knee replacements by finite element simulation. *Proc IMechE, Part H: J Engineering in Medicine* 2012; 226(3): 235–245.

11. Grupp TM, Fritz B, Kutzner I, et al. Vitamin E stabilised polyethylene for total knee arthroplasty evaluated under highly demanding activities wear simulation. *Acta Biomater* 2017; 48: 415–422.

12. Abdelgaied A, Fisher J and Jennings LM. A comprehensive combined experimental and computational framework for pre-clinical wear simulation of total knee replacements. *J Mech Behav Biomed Mater* 2018; 78: 282–291.

13. Kang KT, Son J, Kim HJ, et al. Wear predictions for UHMWPE material with various surface properties used on the femoral component in total knee arthroplasty: a computational simulation study. *J Mater Sci Mater Med* 2017; 28: 105.

14. Abicht C. *Künstliche Kniegelenke nach dem Viergelenkprinzip: Konzeption, Design und tribologische Eigenschaften einer neuen Knieendoprothese mit naturnaher Gelenkgeometrie*. PhD Thesis, Ernst-Moritz-Arndt-Universität Greifswald, Greifswald, 2005.

15. Wohlmuth B. Variationally consistent discretization schemes and numerical algorithms for contact problems. *Acta Numerica* 2011; 20: 569–734.

16. Laursen T. *Computational contact and impact mechanics*. Berlin: Springer, 2002.

17. Maas S, Rawlins D, Weiss J, et al. *FEBio user's manual*. Salt Lake City, UT: The University of Utah, 2016.

18. Gräser C and Sander O. Truncated nonsmooth Newton multigrid methods for block-separable minimization problems. *IMA J Numer Anal* 2018; 39(1): 454–481.

19. Sander O and Jaap P. Solving primal plasticity increment problems in the time of a single predictor-corrector iteration. *Comp Mech* 2020; 65: 663–685.

20. Sander O. *Multidimensional coupling in a human knee model*. PhD Thesis, Freie Universität Berlin, Berlin, 2008.

21. Youett J. *Dynamic large deformation contact problems and applications in virtual medicine*. PhD Thesis, Freie Universität Berlin, Berlin, 2016.

22. Sander O, Klapproth C, Youett J, et al. Towards an efficient numerical simulation of complex 3D knee joint motion. *Comp Vis Sci* 2014; 16(3): 119–138.

23. Blatt M, Burchardt A, Dedner A, et al. The distributed and unified numerics environment, version 2.4. *Arch Numer Soft* 2016; 4(100): 13–29.

24. Bastian P, Buse G and Sander O. Infrastructure for the coupling of Dune grids. In: *Proceedings of ENUMATH 2009*, pp.107–114. Springer. DOI: 10.1007/978-3-642-11795-4_10.

25. The Distributed and Unified Numerics Environment, www.dune-project.org

26. Questmed GmbH. *Mebio: test report TR15-046, 2015*. Kleinmachnow: Questmed GmbH.

27. Endolab GmbH. *Genius pro: test report 42.110530.20. 408, 2011*. Rosenheim: Endolab GmbH.

28. Geuzaine C and Remacle JF. Gmsh: a 3-D finite element mesh generator with built-in pre- and post-processing facilities. *Int J Numer Meth Eng* 2009; 79(11): 1309–1331.

29. Braess D. *Finite elements*. Cambridge: Cambridge University Press, 2007.

30. OpenMP, www.openmp.org

31. Wohlmuth BI and Krause RH. Monotone multigrid methods on nonmatching grids for nonlinear multibody contact problems. *SIAM J Sci Comp* 2003; 25(1): 324–347.

32. Gräser C, Sack U and Sander O. Truncated nonsmooth Newton multigrid methods for convex minimization problems. In: Bercovier M, Gander MJ, Kornhuber R, et al. (eds) *Domain decomposition methods in science and engineering XVIII*. Berlin: Springer, 2009, pp.129–136.

33. Pipping E, Sander O and Kornhuber R. Variational formulation of rate- and state-dependent friction problems. *Zeit Angew Math Mech* 2015; 95(4): 377–395.

34. Archard JF and Hirst W. The wear of metals under unlubricated conditions. *Proc R Sot London, Ser A* 1956; 236(1206): 397–410.

35. Wächter A and Biegler TL. On the implementation of an interior-point filter line-search algorithm for large-scale nonlinear programming. *Math Program* 2006; 106(1): 25–57.

36. Haslinger J and Mäkinen R. *Introduction to shape optimization: theory, approximation, and computation*. Philadelphia, PA: SIAM, 2003.

37. Liu F, Galvin AL, Jin Z, et al. A new formulation for the prediction of polyethylene wear in artificial hip joints. *Proc IMechE, Part H: J Engineering in Medicine* 2010; 225(1): 16–24.

38. Turell M, Wang A and Bellare A. Quantification of the effect of cross-path motion on the wear rate of ultra-high molecular weight polyethylene. *Wear* 2003; 255(7–12): 1034–1039.

39. Strickland MA, Dressler MR and Taylor M. Predicting implant UHMWPE wear in-silico: a robust, adaptable computational-numerical framework for future theoretical models. *Wear* 2012; 274–275: 100–108.